SUPPORTING INFORMATION

Selective Modification and Probing of the Electrocatalytic Activity of Step Sites

Jens Klein, Valeria Chesnyak, Mario Löw, Martin Schilling[1], Albert K. Engstfeld and R. Jürgen Behm*

Institute of Surface Chemistry and Catalysis, Ulm University, D-89069 Ulm, Germany

* Author to whom correspondence should be addressed: juergen.behm@uni-ulm.de
1 Present address: Carl Zeiss SMT GmbH – Zeiss Group, Rudolf-Eber-Str. 2, 73447 Oberkochen, Germany

1. Line profiles

Figure S1 shows apparent height profiles in STM images recorded before and after the CO electro-oxidation. The profiles are along the red line marked in the respective STM image. The STM images are identical with those shown in Figure 1. The apparent height of both the Pt steps (Figure S1a) and the Pt islands (Figure S1b) is 2.26 Å. For Au monolayers on Pt(111) the apparent height is 2.40 Å as determined from Au islands grown on a Pt(111) surface with a submonolayer coverage. The height of a Pt monolayer and a Au monolayer are displayed schematically in the height profiles in Figure S1 by blue and yellow rectangles, respectively. When comparing the height profiles of the STM images recorded before (Figure S1a-d) and after (Figure S1g-j) the CO electro-oxidation, one finds a more pronounced noise in the images recorded after the CO electro-oxidation. We suggest that the larger noise and the different apparent height arise from adsorbates remaining on the surface upon from emersion from the electrolyte.

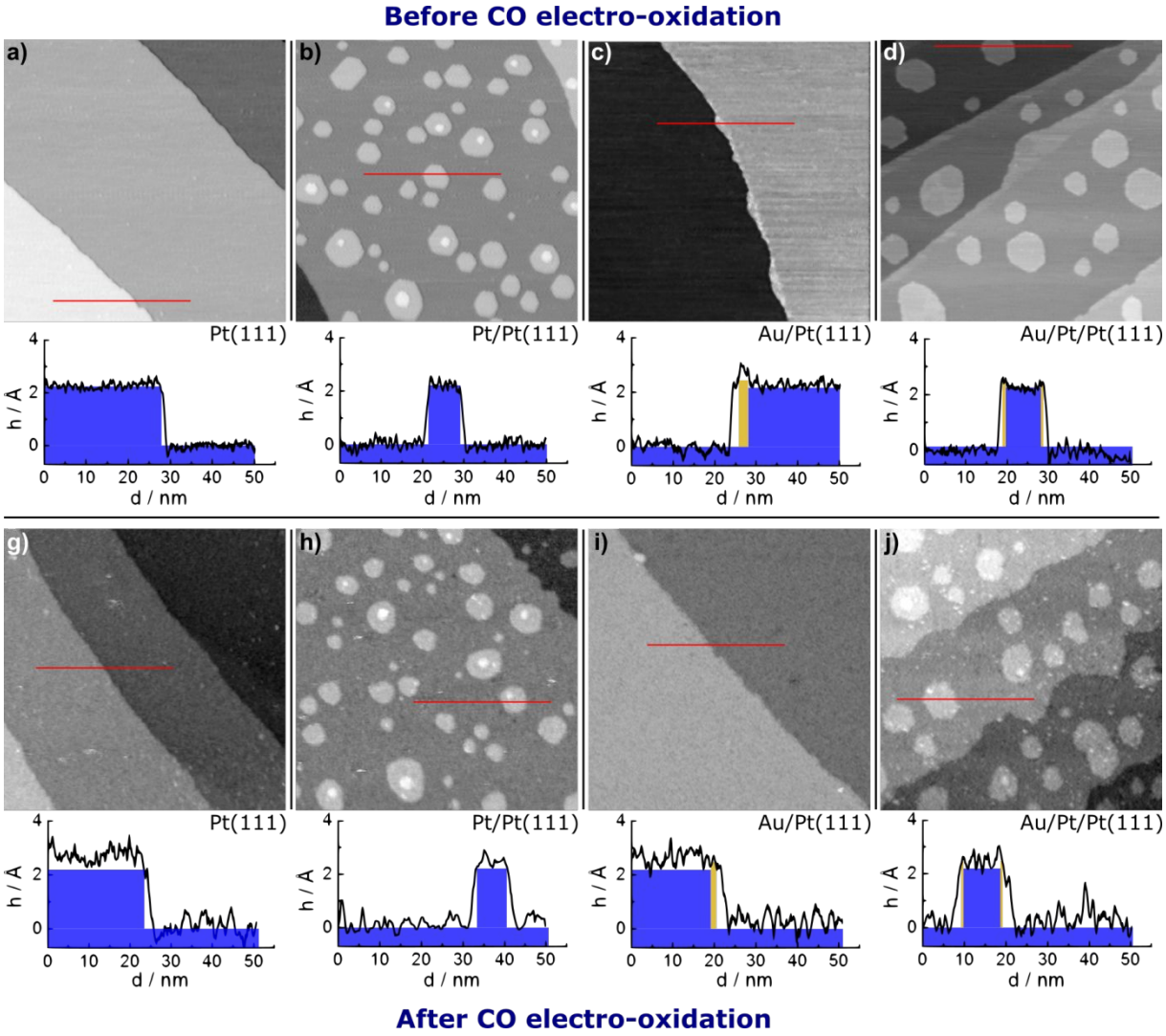

Figure S1: STM images shown in Figure 1 and height profiles along the red lines in the STM image. The blue and yellow rectangles illustrate a monolayer high Pt and Au step / island, respectively.

2. Additional STM images

Additional STM images of the Pt/Pt(111) and Au/Pt/Pt(111) electrodes recorded before the CO electro-oxidation are presented in Figure S2. The island density, the number of bilayer islands and the step density listed in Table 1 were obtained from statistical evaluation of the images in Figure S2, in Figure 1 and from additional images. The STM images of Au/Pt/Pt(111) in Figure S2a and S2b are displayed with enhanced contrast to visualize the Au rim at the Pt island edges.

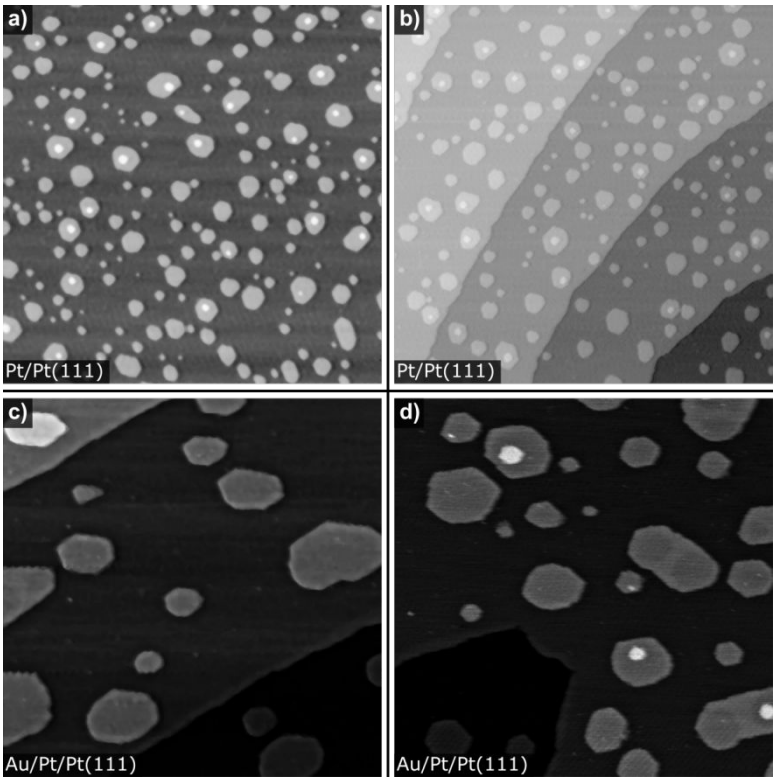

Figure S2: (a) and (b): Additional STM images of Pt/Pt(111). (a): 200 nm x 200 nm, b): 220 nm x 220 nm). (c) and (d): Additional STM images of Au/Pt/Pt(111). (c): 80 nm x 80 nm, b): 100 nm x 100 nm).

3. Electrode surface stability

For Au/Pt(111) and Au/Pt/Pt(111) electrodes with 1 nm - 5 nm narrow stripes of Au at the Pt steps it was not possible to elucidate if the Au films are stable during the bulk CO electro-oxidation, since a chemical contrast was not accessible from STM images recorded after the electrocatalytic reaction. In addition, some surface spots of Au/Pt(111) exhibited bilayer structures at step sites after the CO electro-oxidation which could not be assigned (see Figure S3).

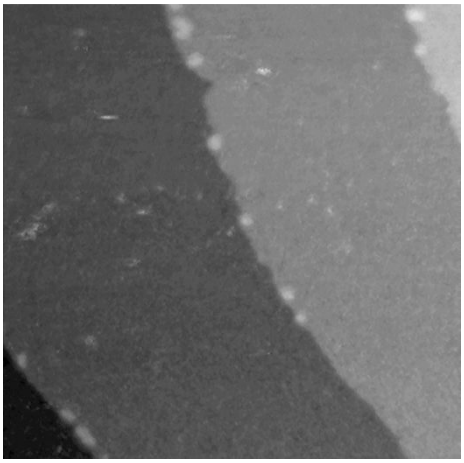

Figure S3: STM image of $Au_{0.07\text{-ML}}$/Pt(111) recorded after the bulk CO electro-oxidation (100 nm x 100 nm, I_T = 5.0 nA, U_T = 0.4 V)

In order to determine the origin of these bilayer islands we prepared Au/Pt(111) electrodes with higher Au coverage (θ_{Au} = 0.30 ML), as shown in representative STM images in Figure S4a and S4d. The stability of the $Au_{0.30\text{-ML}}$/Pt(111) electrode shown in Figure S4a was probed by cyclic voltammetry in 0.5 M H_2SO_4 supporting electrolyte (see Figure S4b). Starting at 0.85 V, the upper potential limit was successively increased in steps of 0.05 V up to 1.10 V. The latter was also the upper potential limit during the bulk CO electro-oxidation. Regardless of the upper potential limit the CVs look essentially identical indicating that in 0.5 M H_2SO_4 the Au films located at the ascending Pt steps remain intact up to 1.10 V. This is evidenced by STM images of $Au_{0.30\text{-ML}}$/Pt(111) recorded after the electrochemical treatment (see Figure S4c).

The stability of the $Au_{0.30\text{-ML}}$/Pt(111) electrode during bulk CO electro-oxidation was probed by measuring three potential cycles in CO saturated 0.5 M H_2SO_4 (see Figure S4e). With consecutive

cycling the absolute current density in the potential regime above the ignition potential increases. STM images recorded after the CO electro-oxidation demonstrate the formation of second layer islands on top of the Au films of $Au_{0.30\text{-ML}}$/Pt(111). As shown in the representative STM image in Figure S4f these second layer islands are solely formed on top of the Au film. Height profiles of the bilayer structures showed that they have an apparent height equivalent to a Au monolayer. Note that despite the formation of second layer Au islands, the ascending Pt steps remain completely modified by a Au film (see Figure S4f). We suggest that this is also the case for small Au coverages as in Figure S3. Since bilayer Au islands were only observed in the presence of CO in the electrolyte solution we suggest that CO might trigger to some extent the detachment of Au atoms from the Au step edge, followed by re-adsorption of Au atoms on top of the monolayer high Au film. A similar behavior was observed previously for the CO adsorption on Pt nanoparticles which are fully encapsulated by a Au film.[1] In the latter study the presence of CO leads to the diffusion of Pt towards the surface due to the thermodynamically favored Pt-CO bond.[1] Thus, we believe that Au atoms at the perimeter of the Au stripes can be forced into the next layer, with the strong Pt-CO bond providing the driving force. This process is however rather slow, and is likely to be inhibited for Au atoms in contact with the Pt steps. The Au adatoms that are forced into the second layer may diffuse on the Au monolayer areas and possibly nucleate 2nd layer islands. However, from the present data it is not possible to derive an exact mechanism. In that case, the increasing absolute current density observed in the high potential region might be explained by the increase in Pt terrace sites accessible for CO electro-oxidation. The results shown in Figure S4 indicate that the bilayer structures observed for $Au_{0.07\text{-ML}}$/Pt(111) in Figure S2 are ascribed to Au bilayers.

Finally, the CO oxidation traces shown in Figure S4e show a hysteresis with a width typical for Au modified Pt(111) electrodes, which is stable also during repeated cycles. This demonstrates that Au removal from the steps is either inhibited or hindered to an extent that the Pt steps are still Au modified. If this were not the case, we would expect that the hysteresis of the Au modified surface increases with increasing cycle number to the value typical for step containing Pt(111) surfaces. The

same observation is found for smaller Au coverages, equivalent to narrower Au decorations, shown below in Figure S7.

Hence, in combination, these findings (from STM and electrochemical measurements) clearly demonstrate that the Au modification at the Pt steps remains stable upon CO electro-oxidation.

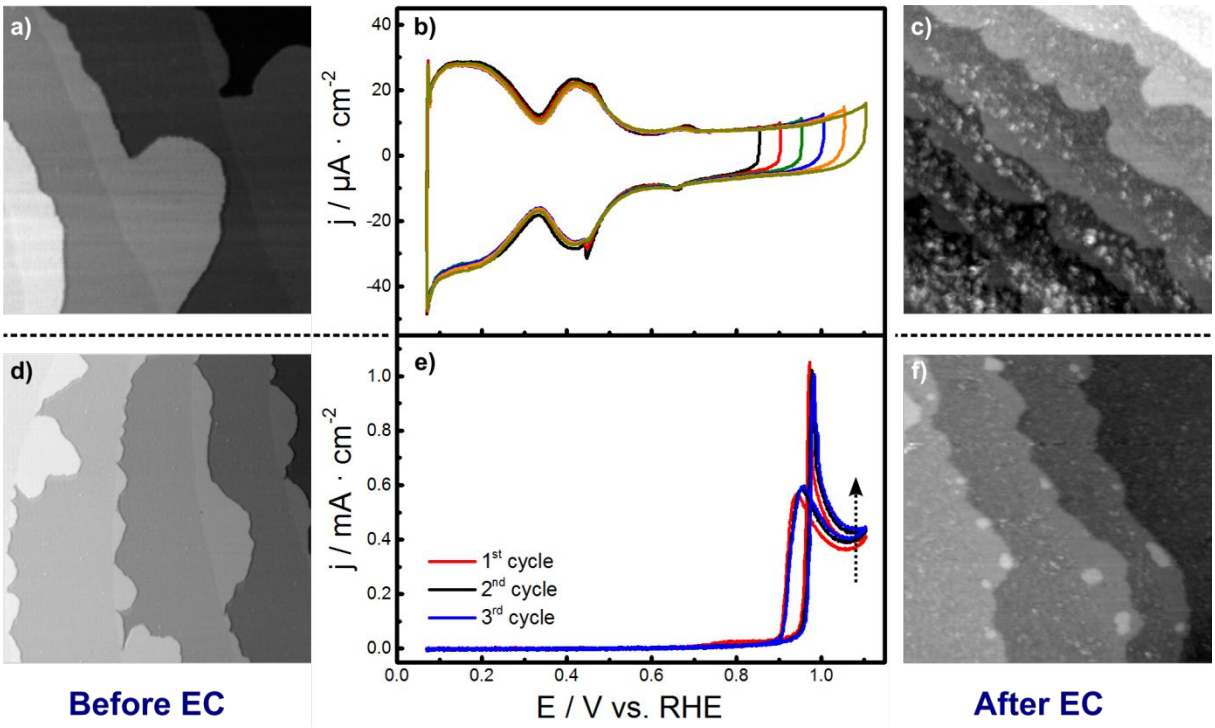

Figure S4: (a) STM image of $Au_{0.30\text{-}ML}$/Pt(111) before EC (100 nm x 100 nm, I_T = 4.5 nA, U_T = 4.5 V). (b) CVs of the $Au_{0.30\text{-}ML}$/Pt(111) shown in a) in 0.5 M H_2SO_4 with increasing upper potential limits (0.05 V to 0.85 V - 1.10 V, 50 mV/s). (c) STM image of $Au_{0.30\text{-}ML}$/Pt(111) after potential cycling in supporting electrolyte up to 1.10 V (100 nm × 100 nm, I_T = 5.0 nA, U_T = 0.01 V). (d) STM image of $Au_{0.30\text{-}ML}$/Pt(111) before EC (300 nm × 300 nm, I_T = 4.5 nA, U_T = 4.5 V). (e) Three consecutive potential cycles during bulk CO electro-oxidation on the $Au_{0.30\text{-}ML}$/Pt(111) electrode shown in d) in CO saturated 0.5 M H_2SO_4 (0.07 V to 1.10 V, 10 mV/s). (f) STM image of $Au_{0.30\text{-}ML}$/Pt(111) after bulk CO electro-oxidation (100 nm × 100 nm, I_T = 5.0 nA, U_T = 0.01 V).

4. CO TPD

CO TPD spectra of CO saturated Pt(111), Pt/Pt(111) and Au/Pt/Pt(111) surfaces are depicted in Figure S5. The small peak around 110 K is attributed to CO desorption from the sample holder. CO desorption from Pt(111) starts at 305 K, followed by an asymmetric peak with a peak maximum at around 400 K. This is in good agreement with previous results and corresponds to a saturation coverage of θ_{CO} = 0.68 ML.[2-5] The CO desorption spectrum of Pt/Pt(111) has an almost identical shape as the one of Pt(111), besides the appearance of a small shoulder at 510 K for Pt/Pt(111), which is attributed to CO desorption from Pt steps.[6] This peak is not present in the CO desorption spectrum of Au/Pt/Pt(111), demonstrating that the Pt steps are no more activated for CO adsorption in the presence of the narrow Au stripe at the ascending step edges. Furthermore, compared to the bare Pt electrodes, CO desorption starts at lower temperatures (280 K) for Au/Pt/Pt(111) and the absolute peak height decreases. Nevertheless, the integrated peak intensity varies only by 2% for the three different surfaces indicating that changes in the CO saturation coverage on the three surfaces are below the detection level. It was shown previously that Pt(111) supported Au films are not available for CO adsorption under these conditions.[7;8] Thus, an identical CO saturation coverage for Au/Pt/Pt(111) and Pt/Pt(111) may at least partly be rationalized by a denser CO adlayer on the Pt terrace sites of the Au modified Pt surface. This would also explain the earlier onset of desorption observed for Au/Pt/Pt(111), since a higher coverage CO adlayer leads to increased repulsive CO – CO interactions, which facilitate the desorption of CO molecules at lower temperature. A higher density CO adlayer on the Pt terrace sites could result from a so-called spillover effect, where the Au film acts as additional channel for CO adsorption onto the Pt terraces, leading to higher saturation coverages on the Pt terrace sites than one would obtain for adsorption on the bare substrate. Based on CO TPD measurements on PtAu/Pt(111) surface alloys, where surface Au and Pt atoms tend to a phase separation, it was already proposed previously that CO molecules that reach Au adsorption sites at the surface may migrate along the surface until they find a Pt adsorption site.[9] Such kind of spillover effect was also reported for CO adsorption on Pt modified Ru(0001) surfaces.[10]

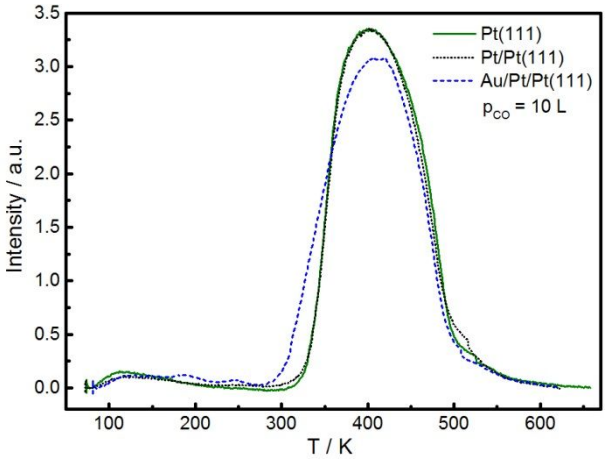

Figure S5: CO TPD spectra of a saturated CO adlayer from Pt(111) (solid green line), Pt/Pt(111) (black dotted line) and Au/Pt/Pt(111) (blue dashed line) with a nominal exposure of ε_{CO} = 10 Langmuir (L).

5. Peak C in the CV of Pt/Pt(111)

So far a peak at 0.31 V (peak **C**) was reported for electrochemically roughened Pt(111).[11] In previous studies, a small shoulder at 0.31 V appeared also in the CVs of Pt(100) [12-16] and Pt(23,1,1) [14] single crystals. For Pt(100) this peak is related to the hydrogen adsorption / desorption on wide (100) terraces.[12;15] As the Pt islands on Pt/Pt(111) grow homoepitaxial, such wide (100) terraces should, however, not be present on the surface of Pt/Pt(111). In CVs of shape-selected Pt nanoparticles (NPs) with cubic or octahedral shape a shoulder was observed at potentials between 0.30 V and 0.37 V.[17;18] Since these NPs have sizes between 8 nm and 12 nm and the number of wide terraces is low, the shoulder should be ascribed to H_{upd} on low-coordination Pt sites. Support for this assumption is the previously observed decrease of the shoulder in the CV of Pt(100) with increasing temperature,[16] since an annealing process should favor larger terraces rather than new defect sites. Thus, we suggest that peak **C** in Figure 2b originates from H/OH adsorption/desorption on low-coordination sites such as kink sites, which have so far not been studied systematically.

6. H_{upd} charges

The overall coulometric charges (Q_{Hupd}) associated with H_{upd} are listed for all electrodes investigated in Table S1. The Q_{Hupd} of Pt(111) is in perfect agreement with previously reported values, it corresponds to a H_{ad} coverage of $\theta(H_{ad}) = 0.66$ ML.[19] The Au modified electrodes exhibit similar Q_{Hupd} values as observed for Pt(111). For Pt/Pt(111) the larger Q_{Hupd} is partly caused by the additional small peaks **A** to **C**, related to Pt defect sites. The total charge density of the peaks **A** to **C** is ca. 5 $\mu C \cdot cm^{-2}$, which corresponds to a contribution of these peaks of approximately 3%. This value is in good agreement with the step density determined from STM imaging.

Table S1. Coulometric charges (Q_{Hupd}) associated with H_{upd}.

Electrode	**Q_{Hupd} / µC cm^{-2}**
Pt(111)	159
Pt/Pt(111)	179
Au/Pt(111)	165
Au/Pt/Pt(111)	161

7. Monolayer high Au film on Pt(111)

A representative STM image of an almost closed monolayer high Au film supported on Pt(111) (Au_{1-ML}/Pt(111)) is shown in Figure S6a. In this case there is no formation of second layer Au islands and the fraction of holes in the Au film is less than 4%. The CV of Au_{1-ML}/Pt(111) in 0.5 M H_2SO_4 supporting electrolyte, which is shown in Figure S6b together with the CV of Pt(111), is in perfect agreement with previously reported CVs for a Au_{1-ML}/Pt(111) electrode.[20] Compared to Pt(111) the H_{upd} region between 0.07 V and 0.33 V almost vanishes for Au_{1-ML}/Pt(111). Furthermore, between 0.33 V and 0.58 V, where sulfate adsorption/desorption is observed on Pt(111), there are solely currents arising from charging of the double layer in the CV of Au_{1-ML}/Pt(111). At potentials above 0.58 V small features are observed, which are related to anion adsorption/desorption as reported for Au(111).[21;22]

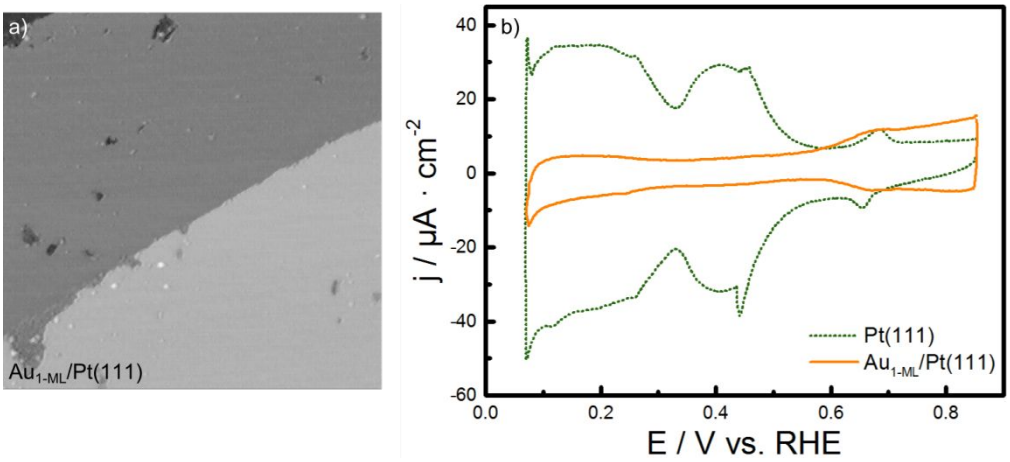

Figure S6: (a) Representative STM image of Au_{1-ML}/Pt(111) (100 nm × 100 nm, I_T = 1.4 nA, U_T = 1.2 V). (b) CVs of Pt(111) (green dotted curve) and Au_{1-ML}/Pt(111) (orange solid curve) in 0.5 M H_2SO_4 (0.07 V to 0.85 V, 50 mV/s).

8. Bulk CO electro-oxidation

The full traces of the first and second polarization curves of the bulk CO electro-oxidation on Pt(111), Pt/Pt(111), Au/Pt(111) and Au/Pt/Pt(111) are shown in the left column of Figure S7. Prior to the ignition region a pre-oxidation feature with small current densities (< 0.05 mA cm^{-2}) is observed in the first polarization curve on all electrodes. This so-called pre-ignition peak was already reported previously and is related to the oxidation of weakly adsorbed CO_{ad} molecules present in the first potential cycle due to a higher density CO_{ad} adlayer.[23-25] The right column of Figure S7 shows the identical polarization curves in the high potential region. Besides negligible deviations the hysteresis width is identical for the first and second cycle for all electrodes.

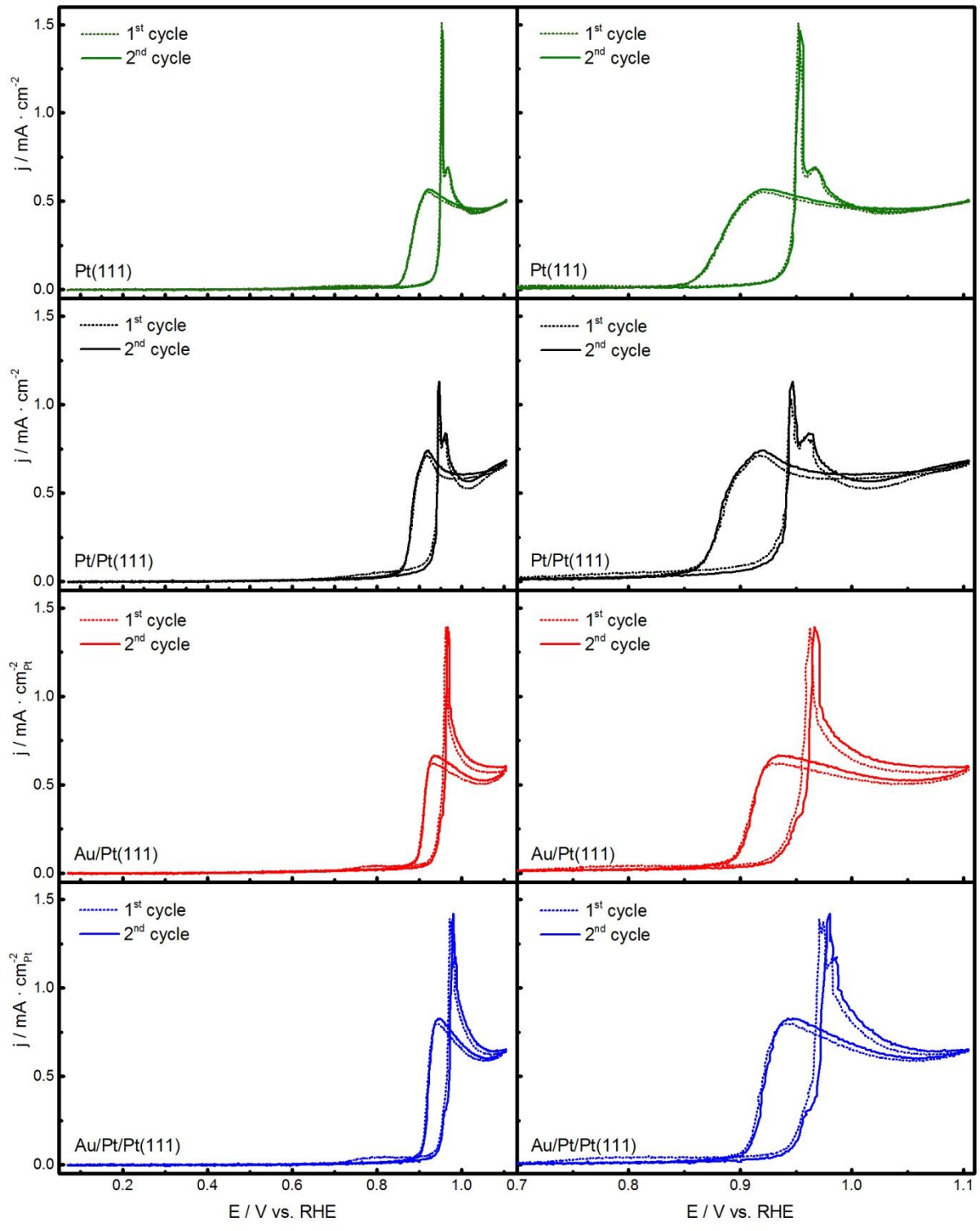

Figure S7: Left column: Full traces of the 1st (dashed curves) and 2nd (solid curves) current density - potential curves of the bulk CO electro-oxidation on (from top to bottom): Pt(111), Pt/Pt(111), Au/Pt(111) and Au/Pt/Pt(111) (0.07 V to 1.10 V, 10 mV/s). Right column: Identical polarization curves as in the left column, but in a smaller potential window (0.70 V to 1.10 V).

9. Sulfate in the CO electro-oxidation

Even though sulfate does not participate in the CO electro-oxidation, its presence may alter the electrode activity due to competitive adsorption with the reactants (here primarily $OH_{ad,}$ since CO binds stronger than sulfate). This has been demonstrated in previous studies, where the hysteresis width in the bulk CO electro-oxidation on Pt(111) was shown to decrease in the presence of strongly binding anions in the electrolyte solution.[26-28] In sulfuric acid the competitive adsorption between OH_{ad} and sulfate starts with the initiation of the CO electro-oxidation.[26] As a result, the OH_{ad} coverage may decrease resulting in lower CO oxidation rates.[26] However, the almost identical shapes of the CVs in Figure 2b demonstrate that the influence of sulfate should be identical for all electrodes investigated regardless of the step density or the Au modification of steps.

10. Electrochemically restructured Pt/Pt(111)

Figure S8a shows CVs in 0.5 M H_2SO_4 supporting electrolyte recorded on an as-prepared Pt/Pt(111) electrode and a Pt/Pt(111) electrode where the surface was exposed to potentials above 1.10 V for several seconds. A potential induced restructuring of the latter electrode is obvious from the presence of distinct peaks in the H_{upd} region, which are ascribed to competitive adsorption / desorption of H / OH at defect sites.[29;30] STM imaging of this restructured Pt/Pt(111) electrode after CO electro-oxidation revealed the formation of small clusters adjacent to small holes in the surface as shown in the inset in Figure S8b. The CV and STM measurements thus indicate the formation of defect rich Pt clusters at the surface. The bulk CO electro-oxidation on the restructured Pt/Pt(111) electrode is shown in Figure S8b. Compared to the polarization curves of Pt/Pt(111) shown in Figure 3, we find a further broadening of the hysteresis width to 80 mV, which we relate to the high amount of defect sites at the surface.

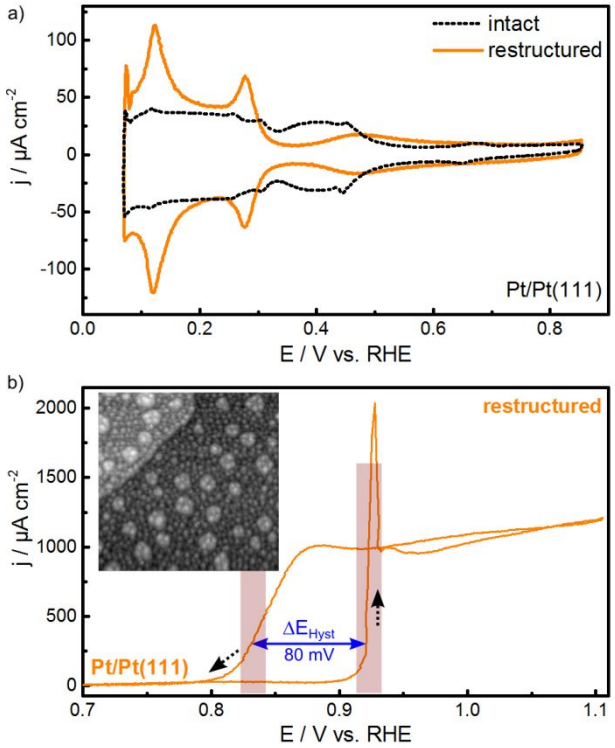

Figure S8: (a) CVs of intact Pt/Pt(111) (black dotted curve) and electrochemically restructured Pt/Pt(111) orange solid curve) in 0.5 M H_2SO_4 (50 mV/s, 0.05 V - 0.85 V). (b) High-potential region (0.70 V - 1.1 V) of the bulk CO electro-oxidation on the restructured Pt/Pt(111) electrode in CO saturated 0.5 M H_2SO_4 (10 mV/s, 0.05 V - 1.10 V). The inset shows an STM image (100 nm × 100 nm, I_T = 2.5 nA, U_T = 0.4 V) recorded after the CO electro-oxidation. ΔE_{Hyst} displays the difference between E_{ign} and the potential in the negative-going scan at j = 0.3 mA cm^{-2}. The faint red bars indicate the experimental accuracy of the potential.

11. Cyclic voltammograms in 0.5 M H_2SO_4

The as-measured CVs of Pt(111), Pt/Pt(111), Au/Pt(111) and Au/Pt/Pt(111) in 0.5 M H_2SO_4 supporting electrolyte are depicted in Figure S9. For the main manuscript the current traces were smoothed by the method of 10 point moving average to lower the signal-to-noise ratio.

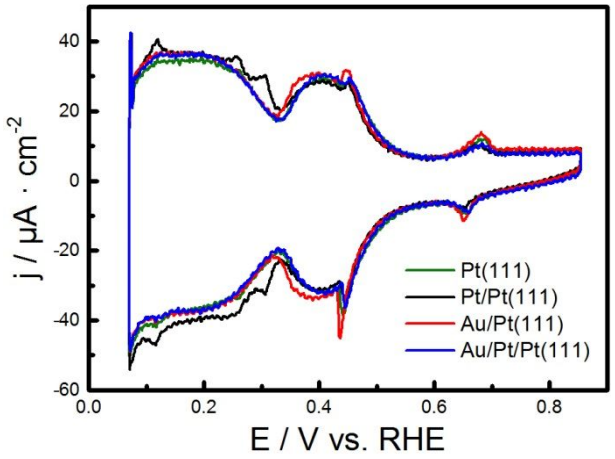

Figure S9: As-measured CVs of Pt(111) (green curve), Pt/Pt(111) (black), Au/Pt(111) (red) and Au/Pt/Pt(111) (blue) in 0.5 M H_2SO_4 (0.07 V to 0.85 V, 50 mV/s).

12. Tunneling parameters

Table S2. Tunneling parameters of STM images shown in Figure 1.

STM image	I_T / nA	U_T / V
Fig. 1a	1.8	1.1
Fig. 1b	1.8	1.1
Fig. 1c	7.9	1.2
Fig. 1d	3.5	1.5
Fig. 1e	3.5	1.5
Fig. 1f	3.5	1.5
Fig. 1g	1.6	0.5
Fig. 1h	7.9	1.2
Fig. 1i	2.0	0.6
Fig. 1j	0.6	1.5

I_T: Tunnel current. U_T: Tunnel voltage.

References

1. Tenney, S. A.; Ratliff, J. S.; Roberts, C. C.; He, W.; Ammal, S. C.; Heyden, A.; Chen, D. A., Adsorbate-Induced Changes in the Surface Composition of Bimetallic Clusters: Pt-Au on TiO2(110), *J. Phys. Chem. C* **2010**, *114*, 21652-21663.

2. Ertl, G.; Neumann, M.; Streit, K. M., Chemisorption of CO on the Pt(111) surface, *Surf. Sci.* **1977**, *64*, 393-410.

3. Gland, J. L.; Kollin, E. B., Carbon monoxide oxidation on the Pt(111) surface: Temperature programmed reaction of coadsorbed atomic oxygen and carbon monoxide, *J. Chem. Phys.* **1983**, *78*, 963-974.

4. Hayden, B. E.; Bradshaw, A. M., The adsorption of CO on Pt(111) studied by infrared reflection-absorption spectroscopy, *Surf. Sci.* **1983**, *125*, 787-802.

5. Schüttler, K. M.; Mancera, L. A.; Diemant, T.; Groß, A.; Behm, R. J., Interaction of CO with Pt_xAg_{1-x}/Pt(111) surface alloys: More than dilution by Ag atoms, *Surf. Sci.* **2016**, *650*, 237-254.

6. Hayden, B. E.; Kretzschmar, K.; Bradshaw, A. M.; Greenler, R. G., An infrared study of the adsorption of CO on a stepped platinum surface, *Surf. Sci.* **1985**, *149*, 394-406.

7. Davies, P. W.; Quinlan, M. A.; Somorjai, G. A., The growth and chemisorptive properties of Ag and Au Monolayers on Platinum single crystal surfaces: An AES, TDS and LEED Study, *Surf. Sci.* **1982**, *121*, 290-302.

8. Skelton, D. C.; Tobin, R. G.; Lambert, D. K.; DiMaggio, C. L.; Fisher, G. B., Oxidation of CO on Gold-Covered Pt(335), *J. Phys. Chem. B* **1999**, *103*, 964-971.

9. Eyrich, M.; Diemant, T.; Hartmann, H.; Bansmann, J.; Behm, R. J., Interaction of CO with Structurally Well-Defined Monolayer PtAu/Pt(111) Surface Alloys, *J. Phys. Chem. C* **2012**, *116*, 11154-11165.

10. Hartmann, H.; Diemant, T.; Behm, R. J., Spill-Over Effects on Bimetallic Pt/Ru(0001) Surfaces, *Top. Catal.* **2013**, *56*, 1333-1344.

11. Jacobse, L.; Huang, Y. F.; Koper, M. T. M.; Rost, M. J., Correlation of surface site formation to nanoisland growth in the electrochemical roughening of Pt (111), *Nat. Mater.* **2018**, *17*, 277.

12. Domke, K.; Herrero, E.; Rodes, A.; Feliu, J. M., Determination of the potentials of zero total charge of Pt(100) stepped surface in the [011] zone. Effect of the step density and anion adsorption, *J. Electroanal. Chem.* **2004**, *552*, 115-128.

13. Furuya, N.; Koide, S., Hydrogen adsorption on platinum single-crystal surfaces, *Surf. Sci.* **1989**, *220*, 18-28.

14. Solla-Gullón, J.; Rodríguez, P.; Herrero, E.; Aldaz, A.; Feliu, J. M., Surface characterization of platinum electrodes, *Phys. Chem. Chem. Phys.* **2008**, *9*, 1359-1373.

15. Vidal-Iglesias, F. J.; Solla-Gullon, J.; Campina, J. M.; Herrero, E.; Aldaz, A.; Feliu, J. M., CO monolayer oxidation on stepped Pt(S) [(n-1)(100)× (110)] surfaces, *Electrochim. Acta* **2009**, *54*, 4459-4466.

16. Zolfaghari, A.; Jerkiewicz, G., The temperature dependence of hydrogen and anion adsorption at a Pt(100) electrode in aqueous H_2SO_4 solution, *J. Electroanal. Chem.* **1996**, *420*, 11-15.

17. Devivaraprasad, R.; Ramesh, R.; Naresh, N.; Kar, T.; Singh, R. K.; Neergat, M., Oxygen Reduction Reaction and Peroxide Generation on Shape-Controlled and Polycrystalline Platinum Nanoparticles in Acidic and Alkaline Electrolytes, *Langmuir* **2014**, *30*, 8995-9006.

18. Vidal-Iglesias, F. J.; Arán-Ais, R. M.; Solla-Gullon, J.; Herrero, E.; Feliu, J. M., Electrochemical Characterization of Shape-Controlled Pt Nanoparticles in Different Supporting Electrolytes, *ACS Catal.* **2012**, *2*, 901-910.

19. Markovic, N. M.; Ross Jr., P. N., Surface science studies of model fuel cell electrocatalysts, *Surf. Sci. Rep.* **2002**, *45*, 117-229.

20. Hazzazi, O. A.; Attard, G. A.; Wells, P. B.; Vidal-Iglesias, F. J.; Casadei, M., Electrochemical characterisation of gold on Pt {h k l} for ethanol electrocatalysis, *J. Electroanal. Chem.* **2009**, *625*, 123-130.

21. Angerstein-Kozlowska, H.; Conway, B. E.; Hamelin, A.; Stoicoviciu, L., Elementary Steps of Electrochemical Oxidation of Single-Crystal Planes of Au - I. Chemical Basis of Processes Involving Geometry of Anions and the Electrode Surface, *Electrochim. Acta* **1986**, *31*, 1051-1061.

22. Angerstein-Kozlowska, H.; Conway, B. E.; Hamelin, A.; Stoicoviciu, L., Elementary Steps of Electrochemical Oxidation of Single-Crystal Planes of Au Part II. A Chemical and Structural Basis of Oxidation of the (111) Plane, *J. Electroanal. Chem.* **1987**, *228*, 429-453.

23. Wieckowski, A.; Rubel, M.; Gutiérrez, C., Reactive sites in bulk carbon monoxide electron-oxidation on oxide-free platinum (111), *J. Electroanal. Chem.* **1995**, *382*, 97-101.

24. Kita, H.; Naohara, H.; Nakato, T.; Taguchi, S.; Aramata, A., Effects of adsorbed CO on hydrogen ionization and CO oxidation reactions at Pt single-crystal electrodes in acidic solution, *J. Electroanal. Chem.* **1995**, *386*, 197-206.

25. Markovic, N. M.; Grgur, B. N.; Lucas, C. A.; Ross, P. N., Electrooxidation of CO and H_2/CO mixtures on Pt(111) in acid solutions, *J. Phys. Chem. B* **1999**, *103*, 487-495.

26. Angelucci, C. A.; Nart, F. C.; Herrero, E.; Feliu, J. M., Anion re-adsorption and displacement at platinum single crystal electrodes in CO-containing solutions, *Electrochem. Commun.* **2007**, *9*, 1113-1119.

27. Malkhandi, S.; Bonnefont, A.; Krischer, K., Strictly potentiostatic current oscillations during bulk CO electro-oxidation on platinum in the presence of inhibiting anions, *Electrochem. Commun.* **2005**, *7*, 710-716.

28. Markovic, N. M.; Lucas, C. A.; Rodes, A.; Stamenkovic, V.; Ross, P. N., Surface electrochemistry of CO and Pt(111): anion effects, *Surf. Sci.* **2002**, *499*, L149-L158.

29. Clavilier, J.; El Achi, K.; Rodes, A., In situ probing of step and terrace sites on Pt (S)-[*n* (111)x(111)] electrodes, *Chem. Phys.* **1990**, *141*, 1-14.

30. Rodes, A.; El Achi, K.; Zamakhchari, M. A.; Clavilier, J., Hydrogen probing of step and terrace sites on Pt (S)-[n (111)x(100)], *J. Electroanal. Chem.* **1990**, *284*, 245-253.